ACS OMEGA

Open Access

http://pubs.acs.org/journal/acsodf

Article

Cryogenic Process Optimization for Natural Gas Purification: Predictive Modeling of Methane−CO_2 Solid−Vapor Phase Equilibrium Using Response Surface Methodology

Anas Ahmed*

Cite This: *ACS Omega* 2024, 9, 27214−27221

Read Online

ACCESS | Metrics & More | Article Recommendations

ABSTRACT: This research combines industrial engineering principles with chemical process modeling to explore the capture of CO_2 from natural gas under cryogenic conditions. The study specifically investigates the Solid−Vapor (S−V) phase equilibrium in a methane−carbon dioxide (CH_4−CO_2) system. The study employs Response Surface Methodology (RSM) to develop a robust model for predicting phase behavior in industrial gas separation processes. The model is validated using experimental data, offering enhanced operational insights into cryogenic CO_2 capture in industrial applications. The developed RSM model is particularly valuable as it can predict the mole fractions of methane and CO_2 at various temperatures and pressures in the solid−vapor region of phase equilibrium, where limited experimental data make it difficult to estimate these components accurately. The key contribution of this study is to validate the RSM model's available experimental data, and the model can further be used to predict the process conditions at which high methane composition (yCH_4) can be achieved. The developed model showed good agreement when the results were compared with previous experimental studies. The utilization of chemical engineering data to forecast previously unknown conditions in gas separation processes broadens the scope of industrial process optimization in this work.

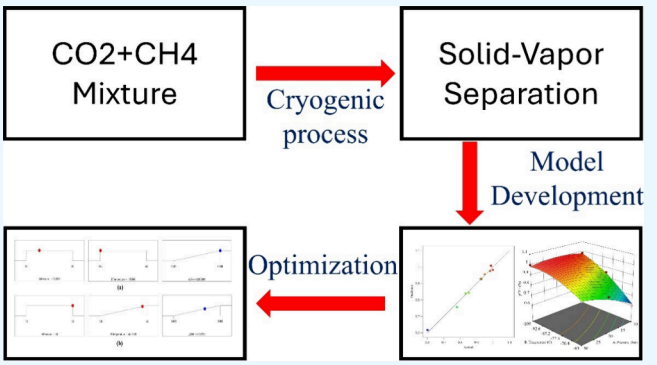

1. INTRODUCTION

The primary problem of the modern era is producing a large amount of CO_2 during energy production from fossil fuels that is not sustainable and viable from environmental and health perspectives.[1] Natural gas emits less carbon dioxide than other fuels synthesized from petroleum, and it is typically considered a cleaner fuel than other fossil fuels. Although this improves its greenhouse effect performance, it may not be completely contaminant-free.[2,3] Before cleaning, natural gas contains several contaminants, including CO_2, H_2S, N_2, etc. Before utilizing natural gas as a fuel, it must be cleaned of its various impurities.[4] One of the main pollutants in natural gas is CO_2, which lowers its energy content and turns acidic and corrosive when in contact with water, damaging pipelines and equipment. CO_2 can harden in LNG processing plants, clogging pipelines, and impeding shipment. As a result, one of the challenging issues with gas separation is the removal of CO_2 from natural gas.[5,6]

Compared to other natural gas processing methods, including membrane, adsorption, and absorption, cryogenic separation is a promising option due to its environmentally friendly operation, as no harmful chemicals are involved during separation. As a viable method for removing CO_2, cryogenic separation has been recognized for many years. However, extensive research into this method was widely believed to be unfeasible due to the large cooling duty.[7] However, recent studies in cryogenic separation have demonstrated that this method can be competitive with alternative technologies with energy integration and careful adjustment of process parameters.[7−12]

Cryogenic could be the first choice due to its advantages, i.e., it is environmentally friendly, has physical separation without any harmful solvents, and is applicable for a large range of compositions of natural gas with CO_2.[13,14] However, many challenges still exist because it requires a substantial cooling duty.[15] Achieving the low temperatures necessary for efficient phase separation requires significant energy requirements, often leading to an expensive process. This energy-intensive process also escalates operational costs and complicates the economic viability of cryogenic methods.[16] Furthermore, the cryogenic process infrastructure must endure severe thermal conditions,

Received: February 16, 2024
Revised: May 26, 2024
Accepted: May 29, 2024
Published: June 10, 2024

necessitating advanced materials and precision control mechanisms and elevating the initial capital outlay and maintenance complexity. The need for precise control of thermodynamic parameters highlights the importance of strict design and operational standards. These factors collectively highlight the imperative for innovative research to enhance the energy efficiency of cryogenic CO_2 capture processes and align them with the overarching objectives of sustainable development in natural gas processing.[17,18]

Cryogenic separation is categorized into three main fields based on the different separation mechanisms by Khurram et al., which are (i) Conventional, (ii) Nonconventional, and (iii) Hybrid.[19] However, one thing common in all three technologies is the involvement of high pressure and low temperature, which needs to be carefully tuned to reduce energy consumption and make it a strong competitor with other technologies.[7,20]. Conventional cryogenic separation comprises cryogenic distillation, in which separation occurs in the liquid−Vapor (L-V) region of phase equilibria. This field of research is well established, and a good amount of data is available. Nonconventional separation involves separation in the solid−vapor region of phase equilibria, which is also the scope of this study. The hybrid is the combination of conventional and nonconventional in which separation occurs in the solid−liquid−vapor (S-L-V) region.

Nonconventional cryogenic separation suffers from the shortage of experimental data in the literature that addresses the quantitative study of CO_2 solidification, which is essential information for choosing the best process parameters. Additionally, most of the predicted data is generated from process simulators or other thermodynamic models;[21,22] the reliability of these simulators is not fully established and hinges on the precise application of both the thermodynamic models and the experimental data. Furthermore, certain thermodynamic models may incur substantial computational demands due to their analytical complexity. The efficacy of process simulators is still debatable and depends on their proper application to experimental data and thermodynamic models. On the other hand, thermodynamic models require longer calculation times due to their analytical complexity.[23]

Recently, Ali et al. developed ANN-based techniques to predict the phase behavior of CO_2 and CH_4 systems with various temperatures and pressures.[24] Despite the promising results, the temperature range was constrained and did not include the whole phase equilibrium region due to the restricted amount of available experimental data.

Based on the limited availability of data, developing a simple yet accurate technique to predict phase behavior is necessary. RSM could be a good choice, because it is straightforward and reasonable. Response Surface Methodology (RSM) is used in this work to accurately predict phase behavior over a wide range of pressures and temperatures. Regarding the predictive modeling of the methane-carbon dioxide solid−vapor phase equilibrium, RSM is more straightforward and streamlined than process simulators and intricate thermodynamic models, making it easier to optimize process parameters with fewer experimental runs.[25] RSM can generate precise models with fewer experimental data.[26] It can play a crucial role in cryogenic separation, especially in cases where obtaining comprehensive experimental data is often challenging.[27]. The efficiency of the RSM in model development, requiring fewer experiments, addresses the challenges posed by resource-intensive and technically demanding cryogenic experiments.

The cryogenic systems stay at optimal throughout various possible operational situations because of the robust and resilient nature of the designs created by RSM, which also considers process variability and uncertainties. In cryogenic separation, where even small differences in the temperature or pressure parameters can result in major variations in process efficiency and product quality, it is imperative to retain this robustness.

This study uses RSM to predict the phase behavior of CH_4 and CO_2 binary systems for a wide temperature and pressure range. Moreover, the optimum conditions were investigated to separate these two components, with minimum methane losses and maximum CO_2 capture. This study could help design an S−V-based cryogenic separation system for naturally efficient gas purification with minimum energy requirements.

2. METHODOLOGY

The experimental data used to develop the model was from cited literature.[24,28] The design of the experiment was employed to generate the relation between the input and output parameters. Figure 1 illustrates the qualitative phase equilibrium of a CO_2−CH_4 binary mixture at a constant composition under varying pressure and temperature conditions. The area under investigation in this study is vapor−solid, as shown in Figure 1. As per the phase rule, a system with one degree of freedom ($F = 1$) is termed univariant and is depicted as lines on a phase diagram, while a system with two degrees of freedom ($F = 2$) is bivariant, represented by areas on the diagram. Figure 1 illustrates that the solid phase consists of pure CO_2 in the vapor−solid region. This is supported by Donnelly and Katz, who noted that the melting point of the solid in this region aligns with the melting point of CO_2, confirming its purity. In the liquid−solid region, partial dissolution of solidified CO_2 occurs in the liquid phase. Lastly, the solid−solid region indicates that the solidified CO_2 remains stable and that the liquid phase will eventually solidify under sufficiently extreme conditions.

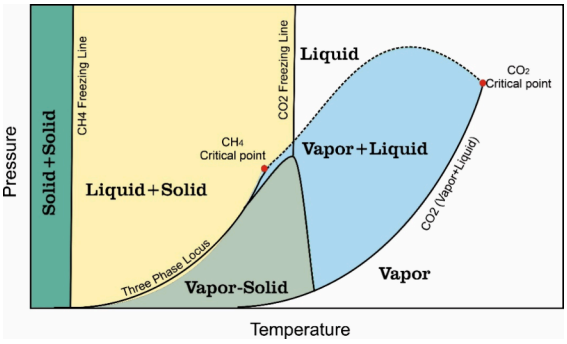

Figure 1. General phase diagram for methane and carbon dioxide at constant composition across pressure and temperature conditions.

This study examines the effect of temperature and pressure (input parameters) interaction on the composition of CH_4 in the vapor phase (yCH_4) by using DoE and face-centered central composite design (CCD). Table 1 shows the input parameters and the response. The empirical correction between input and responses was developed using RSM. It is a well-known modeling method for developing the relationship between inputs and responses. It investigates the effect of the most and least dominant elements on the response, making it an effective tool for modeling and optimization.[25]

https://doi.org/10.1021/acsomega.4c01526
ACS Omega 2024, 9, 27214−27221

Table 1. DoE Table of Inputs and Response[a]

Sr. No.	Pressure (bar)	T (°C)	yCH_4 (%)
1	30	−63	0.832
2	10	−63	0.601
3	10	−100	0.982
4	20	−81.5	0.92
5	20	−81.5	0.927
6	20	−100	0.987
7	30	−100	1
8	10	−81.5	0.853
9	20	−63	0.78
10	30	−81.5	0.948

[a]Adapted with permission from ref 28. Copyright 1959 The Author.

3. RESULTS AND DISCUSSION

3.1. Model Development. Table 1 summarizes the CCD matrix, design details, factors, and responses. Equation 1 shows a second-order quadratic polynomial regression model that links the response, yCH_4, with interactions between the pressure and temperature.

$$yCH_4 = 0.04083P - 0.03434T + 0.00029PT - 0.00028P^2 - 0.000128T^2 - 1.213 \quad (1)$$

In eq 1, P and T represent the pressure and temperature, respectively.

ANOVA was utilized for the quadratic polynomial model to assess the significance of the model and its constituent factors. This statistical method generated values for degrees of freedom, sum of squares, and mean squares for each factor. A factor is deemed significant within the 95% confidence interval set by the RSM if either (1) its F-value is substantial or (2) its associated p-value is below the threshold of 0.05; factors not meeting these criteria are considered insignificant. The detailed ANOVA findings are presented in Table 2.

Table 2. Analysis of Variance (ANOVA) for the Relationship Between Pressure and Temperature on the Response Variable

Source	Sum of squares	df	Mean squares	F values	P values
Model	0.1338	5	0.0267	61.07	0.0007
A-Pressure	0.0194	1	0.0194	44.48	0.0026
B-Temperature	0.0947	1	0.0947	216.2	0.0001
AB	0.0115	1	0.0115	26.37	0.0068
A^2	0.0019	1	0.0019	4.368	0.1048
B^2	0.0048	1	0.0048	11.09	0.0290
Residual	0.0017	4	0.0004	61.07	
Lack of Fit	0.0017	3	0.0005	44.48	
Pure Error	0	1	0		
Cor Total	0.1355	9			

The ANOVA results indicate a model of high significance, underscored by a model F-value of 61.07. Such an F-value, corresponding to a model P-value of 0.0007, implies a negligible 0.07% probability that this result could arise from random data variation, affirming the model's substantial explanatory power. Significance levels, as determined by P-values, reveal that factors with values below 0.0500 significantly impact the dependent variable. Specifically, pressure (A), temperature (B), their interaction (AB), and the quadratic term for temperature (B^2) significantly contribute to the model. In contrast, P-values exceeding 0.1000, such as the P-value for the quadratic term of pressure (A^2), suggest nonsignificant contributions.

The identified nonsignificant terms, excluding those required for the hierarchical integrity of the model, hint at the possibility of refining the model. The model's simplicity and interpretability could be enhanced by eliminating these terms without diminishing its explanatory strength. The ANOVA substantiates that the model effectively delineates the relationship between the dependent variable and the independent factors—pressure and temperature—both individually and interactively. The substantial F-value coupled with the low P-values for pivotal model terms corroborates the model's robustness. Moreover, the nonsignificant quadratic term for pressure (A^2) indicates an opportunity to streamline the model for increased efficiency.

The statistical metrics indicate a strong regression model with a standard deviation of 0.0209 and a coefficient of variation of 2.37%, reflecting a high precision and low relative variability (Table 3). The R-squared value of 0.987 suggests that the model

Table 3. Summary of Regression Model Diagnostics and Fit Statistics

Standard Deviation	0.0209
Mean	0.8835
C.V. %	2.37
R^2	0.9871
Adjusted R^2	0.9709
Predicted R^2	0.8570
Adequate precision	24.0964

explains 98.7% of the variability in the response variable, with an adjusted R-squared of 0.971 accounting for the number of predictors. The predicted R-squared of 0.857 indicates that the model is expected to predict new data well, and an adequacy precision ratio of 24.10 confirms the model's capability to distinguish between signal and noise. These values collectively suggest that the model is accurate and reliable for prediction.

3.2. Model Adequacy Tests. The developed model is subjected to adequacy tests using several tests. The first test is a normal probability plot of externally studentized residuals, a diagnostic tool used in regression analysis to assess the normality of the residuals (Figure 2). It is evident from the figure that the majority of the data points closely align with the reference line in the normal probability plot, indicating the residuals' conformity to a normal distribution. This alignment is particularly strong in the central region of the plot, which is the most critical area for assessing the normality. The minor deviations observed at the tails are typical in statistical data and do not significantly detract from the overall normal distribution of the residuals.

The externally studentized residuals are plotted against the values that the developed regression model predicted in Figure 3. A fundamental assumption in regression analysis known as homoscedasticity is tested using this kind of plot: whether the residuals or the discrepancies between observed and projected values exhibit consistent variance over the range of predictions. The plot indicates that the residuals form no particular pattern, scattered randomly around the zero line. Given that the variance of the residuals appears to be constant for all projected values, this random dispersion shows that our model satisfies the homoscedasticity requirement.

The regression model is stable and reliable throughout a wide range of predictions, as demonstrated by the constant residual

https://doi.org/10.1021/acsomega.4c01526
ACS Omega 2024, 9, 27214−27221

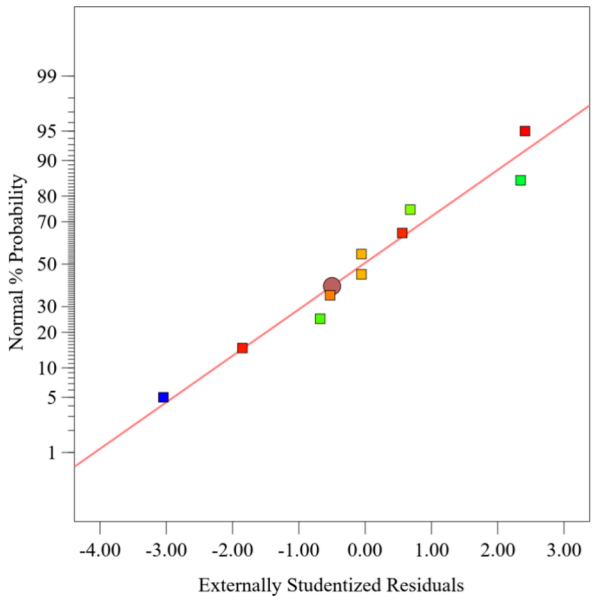

Figure 2. Normal probability plot of externally studentized residuals.

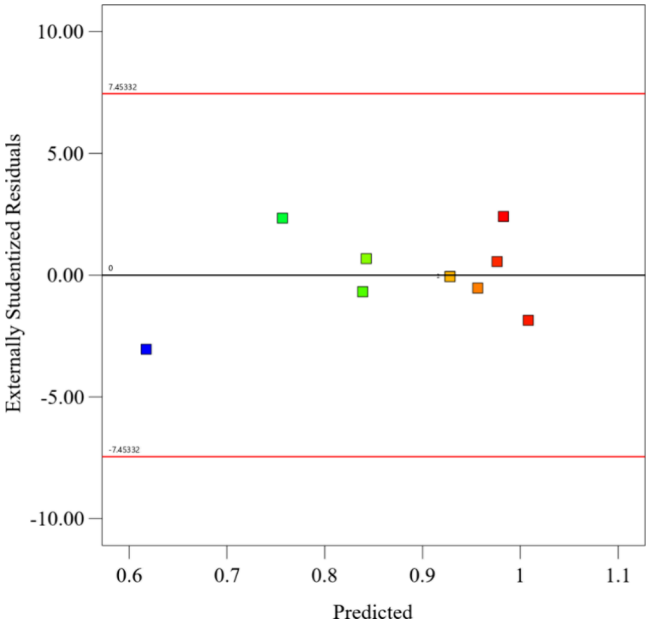

Figure 3. Externally studentized residuals vs predicted values.

spread in this figure, which supports the model's application to further predictive tasks. This plot's lack of patterns or trends indicates that the model fits the data well.

A run chart of the externally studentized residuals for each observation in the regression analysis is shown in Figure 4, plotted against the run number. This kind of chart helps see trends over time or in the sequence of the runs, which may point to possible model issues like nonrandom errors or trends related to time. Ideally, the residuals should be dispersed randomly around the zero line and should not exhibit any systematic patterns pointing to a possible flaw in the model's assumptions. The plot indicates no discernible pattern or trend in the residuals' oscillations above and below the zero line, indicating that neither time nor run order contradicts the model's assumptions.

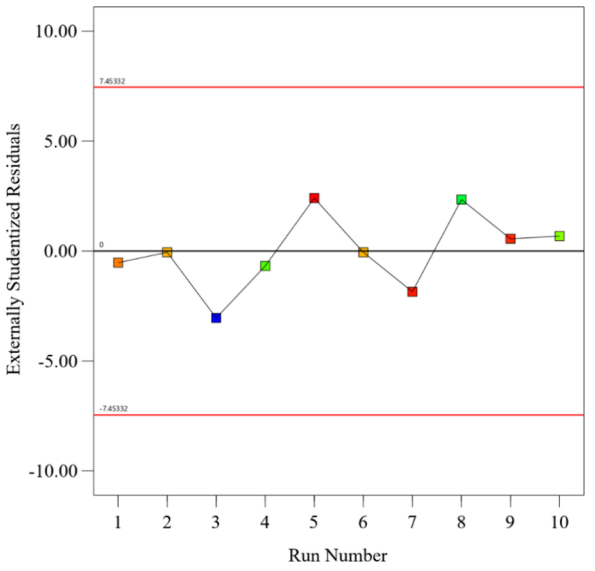

Figure 4. Run chart of externally studentized residuals across sequential runs.

As expected from a well-fitting regression model, the lack of patterns in Figure 4 shows that the residuals are independent and identically distributed. This absence of seasonality or trend indicates that the model correctly represents the underlying process, hence confirming the model's predictive validity for new observations.

Figure 5 illustrates a Cook's distance plot employed to detect influential observations in the regression model. Cook's distance

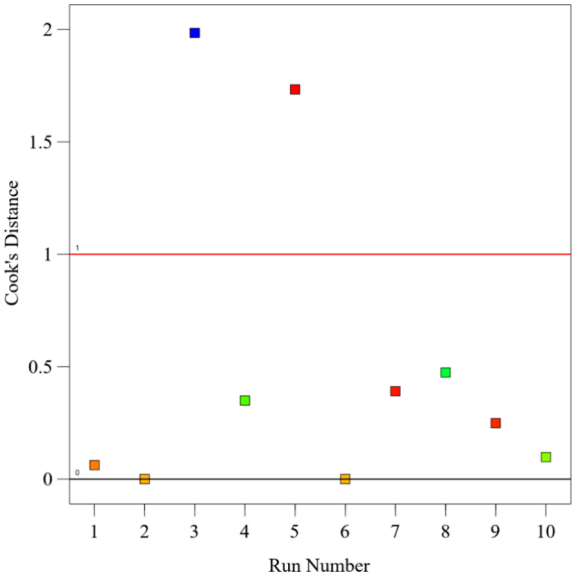

Figure 5. Cook's distance vs run number to identify influential points in the regression model.

measures the effect of deleting a single observation. Points with a Cook's distance larger than 1 (as indicated by the horizontal red line) are typically considered influential.

In this graph, the horizontal axis represents the run number, which corresponds to each data point in the analysis, and the vertical axis denotes the Cook's distance for each of these points. Most data points lie below the threshold, indicating that they do not influence the model's parameters. However, a few points

https://doi.org/10.1021/acsomega.4c01526
ACS Omega 2024, 9, 27214−27221

above the threshold suggest that those particular runs have a more substantial influence on the model and may warrant further investigation.

Identifying these points is crucial, because their exclusion from the model could significantly alter the results. The figure indicates that while most data points do not excessively influence the model, a select few could be pivotal and thus merit closer scrutiny in the context of the model's robustness and the reliability of its predictions.

Figure 6 provides a scatter plot comparing the predicted values from the regression model to the actual observed values.

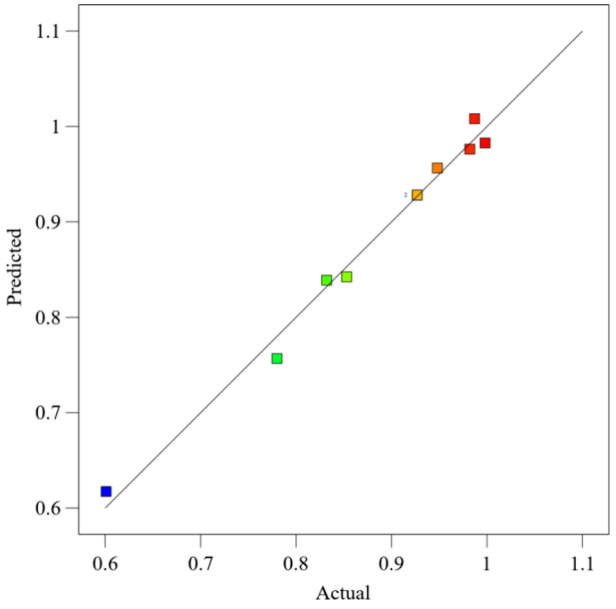

Figure 6. Validation of model using experimental data.

The proximity of the data points to the diagonal line indicates the model's predictive accuracy. The closer the points lie to this line, the more accurate the model's predictions are.

In this case, the data points are generally close to the line, suggesting that the model's predictions agree with the actual values. This demonstrates the model's effectiveness in capturing the underlying relationship between the studied variables. The plot confirms its capacity to predict the response variable accurately. Such a plot is essential for evaluating the model's performance and identifying systematic deviations between the predicted and actual values.

Figure 7 shows the 3D surface plots among the temperature, pressure, and CH_4 composition in a vapor phase. Surface plots are the best representation of graphs that show the combined effect of input parameters and response. It can be observed from Figure 4 that at high temperatures and low pressure, the quantity of methane in vapor was minimal. While at low temperature and high pressure, it was the maximum. The surface color gradient, ranging from green at lower values to red at higher values, represents the increase in the methane mole fraction with changes in temperature and pressure. This type of visualization is crucial for identifying the combined effect of the two independent variables on the response variable. The overlay of the surface's experimental data points (red dots) allows for direct comparison between the model's predictions and observed values.

The plot helps assess the adequacy of the model in capturing the nonlinear relationships and interaction effects between the

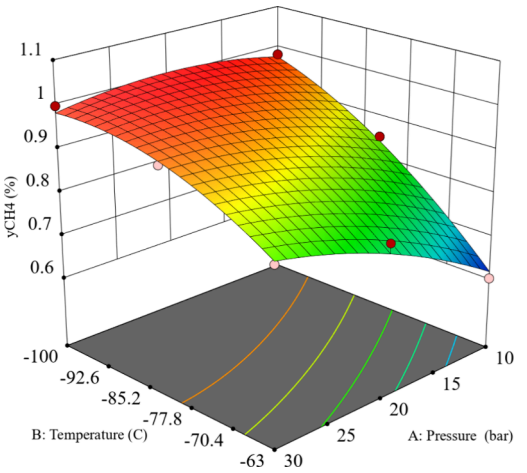

Figure 7. 3D surface plot showing the relationship between temperature, pressure, and CH_4 mole fraction.

temperature and pressure on methane production. It serves not only as a tool for model validation but also as a guide for optimizing the conditions to achieve the desired outcomes in methane production. The minimum quantity at low pressure and high temperature is due to the very low liquefaction point of methane, which is around −160 °C.

3.3. Model Validation. The model's predictive accuracy was further evaluated using additional experimental data presented in Figure 8. In Figure 8a, the scatter plot compares the experimental data from Xiong et al.[29] and the predicted values obtained from RSM. Compared to the experimental results, the coefficient of determination R^2 = 0.9501 demonstrates a significant correlation and high predicted accuracy for the RSM.

Figure 8b compares the experimental findings from Agarwal et al.[30]. With R^2 = 0.9324, the results show a fair agreement between the experimental and predicted data. Even though this R^2 is marginally lower than the one found using Xiong's data.[29], the RSM has a significant predictive power. The charts show the degree to which the RSM can predict the experimental results of Xiong and Agarwal. The fair R^2 values in both graphs demonstrate the practical usability and dependability of the RSM for the field prediction analysis.

3.4. Optimization Case Studies. Figure 9 illustrates the modeled relationship between the temperature (B), pressure (A), and the resulting methane mole fraction. The contour lines represent methane concentration levels, with the color gradient indicating increasing levels from blue (low) to red (high). The plot is particularly useful for visualizing the optimal conditions for maximizing methane production within the experimental design space.

The limitations for optimizing methane production are listed in Table 4. Temperature (B) ranges are −100 °C and −63 °C, and pressure (A) is between 10 and 30 bar. Due to an equivalent importance, a weighting of 3 indicates strong relevance in the optimization process. The objective of the methane mole fraction (yCH_4) is to maximize it within the defined feasible region with a specified range between 0.601% and 0.998%. The constraints are equally weighted, indicating a balanced approach to optimization where the pressure, temperature, and methane concentration are all equally important. These parameters are critical for guiding the optimization algorithm to find the most productive conditions within specified ranges.

https://doi.org/10.1021/acsomega.4c01526
ACS Omega 2024, 9, 27214−27221

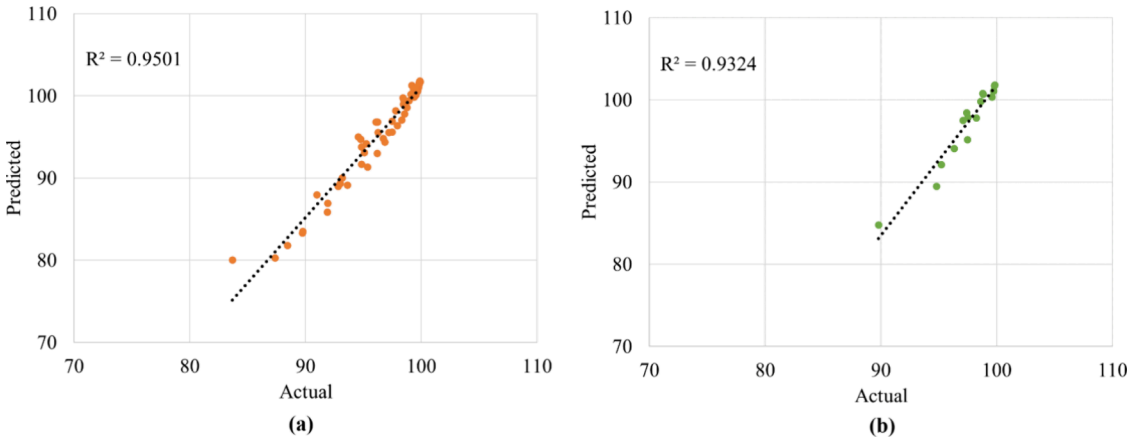

Figure 8. Model validation using experimental data of (a) Xiong et al.[29] and (b) Agarwal et al.[30]

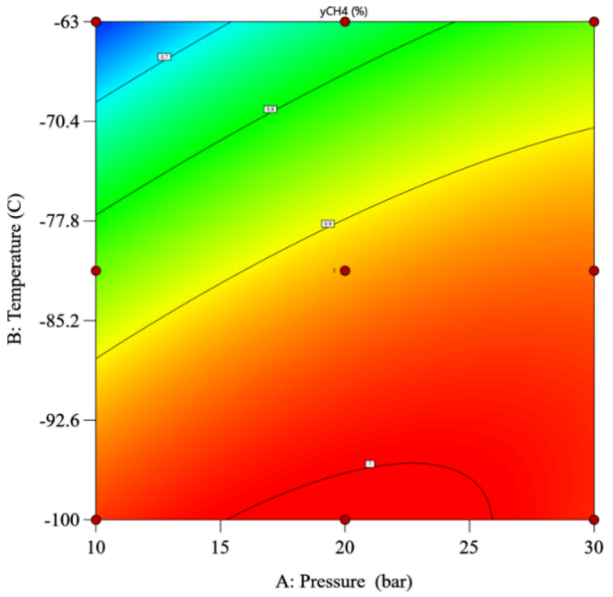

Figure 9. Contour plot of methane mole fraction yCH_4 (%).

The optimization study explored two distinct case scenarios to maximize the methane mole fraction (yCH_4). In the first case study, the temperature and pressure parameters were kept within their specified ranges without exerting additional influence on the outcomes. However, The second case study focused on maintaining the pressure within the designated range while maximizing the temperature. This approach aimed to achieve high-purity methane (CH_4) with a minimum cooling duty. These case studies were integral in determining the most effective conditions for methane production optimization.

Figure 10 presents case study 1 (a) and case study 2 (b) outcomes, depicted as ramp functions. Figure 10a demonstrates that a high methane purity of 99.98% is achievable at the conditions of −99.5 °C and 15.7 bar, with the temperature at its lower boundary and the pressure at a moderate level. These conditions favor applications requiring high methane purity, such as in Liquefied Natural Gas (LNG) production. On the other hand, case study 2 Figure 10b shows a lower methane purity of 86.7% at −66.4 °C and 30 bar. This set of conditions may be appropriate for scenarios in which a lower methane purity is acceptable. Notably, the temperature in case study 2 is close to the upper limit of the specified range, suggesting that less cooling is required to achieve the desired methane purity.

CONCLUSION

The RSM-based model was developed to predict the phase behavior of the CH_4−CO_2 binary system and the vapor composition of CH_4 in a cryogenic separator. The results indicated increased methane vapor presence at lower temperatures and higher pressures with CO_2 predominantly in the liquid phase. Conversely, the opposite behavior was observed at high temperatures and lower pressure. Two input parameters, pressure and temperature, were selected to investigate their effect on the CO_2 capture efficiency. The pressure and temperature ranges for the study were selected: 10 to 30 bar and −63 to 100 °C. The model was validated using two different sets of experimental data, and the agreement was good, with R^2 values of 0.9501 and 0.9324. Lastly, the study examined two case studies to determine the conditions for maximizing the methane purity in a CH_4−CO_2 system, contributing to the broader application of cryogenic technology for the capture of CO_2 from natural gas. In case study 1, the methane composition reaches approximately 99.99% at a pressure of 15.7059 and a temperature of −99.546. In contrast, in case study 2, the composition is approximately 86.72% at a pressure of 30 and a temperature of −66.3849. This work could help design an S−V-based cryogenic separator that requires minimum energy.

Table 4. Constraints for Optimization

	Name	Goal	Lower limit	Upper limit	Lower weight	Upper weight	Importance
Case study 1	pressure	in range	10	30	1	1	3
	temperature	in range	−100	−63	1	1	3
	yCH_4	maximize	0.601	1	1	1	3
Case study 2	pressure	in range	10	30	1	1	3
	temperature	maximize	−100	−63	1	1	3
	yCH_4	maximize	0.601	1	1	1	3

https://doi.org/10.1021/acsomega.4c01526
ACS Omega 2024, 9, 27214−27221

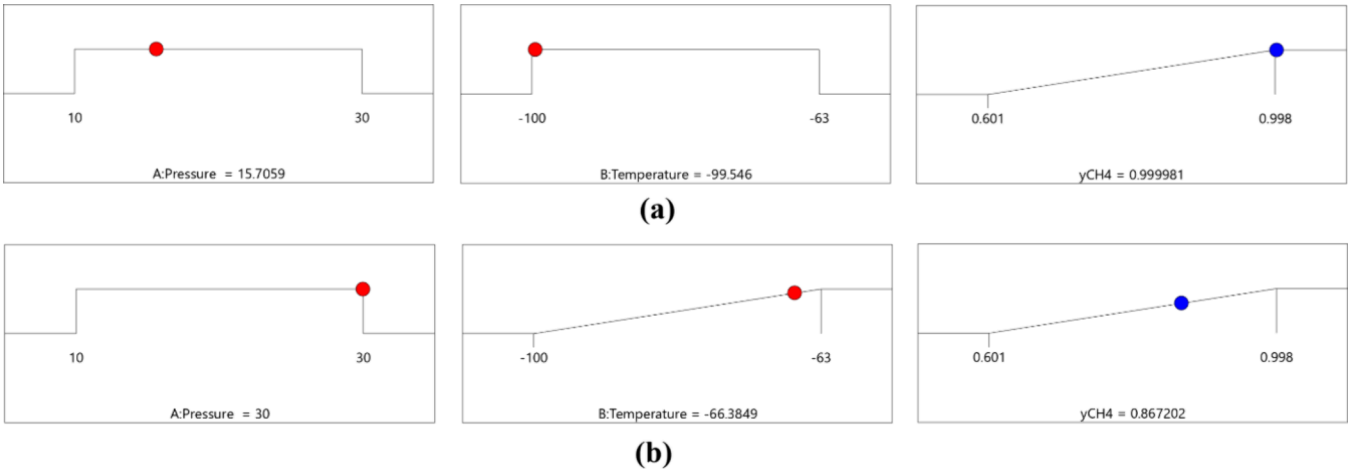

Figure 10. Ramp function of two optimization case studies: (a) input in designated range, (b) pressure in designated range while temperature is maximized.

AUTHOR INFORMATION

Corresponding Author

Anas Ahmed − *Department of Industrial and Systems Engineering, University of Jeddah, Jeddah 23890, Saudi Arabia*; Email: aahmed5@uj.edu.sa

Complete contact information is available at: https://pubs.acs.org/10.1021/acsomega.4c01526

Notes

The author declares no competing financial interest.

ACKNOWLEDGMENTS

This work was funded by the University of Jeddah, Jeddah, Saudi Arabia, under grant No. UJ-22-DR-10. The authors, therefore, acknowledge with thanks the University of Jeddah for technical and financial support.

REFERENCES

(1) Shimekit, B.; Mukhtar, H. Natural Gas Purification Technologies−Major Advances for CO_2 Separation and Future Directions. In *Advances in Natural Gas Technology*; IntechOpen, 2012; Vol. *2012*, pp 235−270.

(2) Moreira, M. A.; Ribeiro, A. M.; Ferreira, A. F.; Rodrigues, A. E. Cryogenic Pressure Temperature Swing Adsorption Process for Natural Gas Upgrade. *Separat. Purif. Technol.* **2017**, *173*, 339−356.

(3) Ali, A.; et al. Synthesis and mixed integer programming based optimization of cryogenic packed bed pipeline network for purification of natural gas. *Journal of Cleaner Production* **2018**, *171*, 795−810.

(4) Font-Palma, C.; Cann, D.; Udemu, C. J. C. Review of cryogenic carbon capture innovations and their potential applications. *C* **2021**, *7* (3), 58.

(5) Wilson, E. F. A Review on the Use of Natural Gas Purification Processes to Enhance Natural Gas Utilization. *Int. J. Oil, Gas Coal Eng.* **2022**, *11*, 17−27.

(6) Yang, H.; Xue, L.; Yang, X.; Xu, H.; Gao, J. Advances in metal-organic frameworks for efficient separation and purification of natural gas. *Chinese Journal of Structural Chemistry* **2023**, *42* (2), 100034.

(7) Hart, A.; Gnanendran, N. J. E. P. Cryogenic CO_2 capture in natural gas. *Chinese Journal of Structural Chemistry* **2009**, *1* (1), 697−706.

(8) Tuinier, M. J.; van Sint Annaland, M.; Kuipers, J. A. M. A novel process for cryogenic CO_2 capture using dynamically operated packed beds—An experimental and numerical study. *International Journal of Greenhouse Gas Control* **2011**, *5* (4), 694−701.

(9) Tan, H.; Ding, Z.; Wen, N. J. A. T. E. Numerical study on the thermodynamic performance of a packed bed cryogenic energy storage system. *Appl. Therm. Energy* **2022**, *214*, 118903.

(10) Ali, A.; Maqsood, K.; Syahera, N.; Shariff, A. B.; Ganguly, S. Energy minimization in cryogenic packed beds during purification of natural gas with high CO2 content. *Chem. Eng. Technol.* **2014**, *37* (10), 1675−1685.

(11) Northrop, P. S.; Valencia, J. A. J. E. P. The CFZ process: A cryogenic method for handling high-CO2 and H2S gas reserves and facilitating geosequestration of CO2 and acid gases. *Energy Procedia* **2009**, *1* (1), 171−177.

(12) Maqsood, K.; Ali, A.; Shariff, A. B.; Ganguly, S. Process intensification using mixed sequential and integrated hybrid cryogenic distillation network for purification of high CO_2 natural gas. *Chem. Eng. Res. Des.* **2017**, *117*, 414−438.

(13) Chang, H.-M. J. C. A thermodynamic review of cryogenic refrigeration cycles for liquefaction of natural gas. *Cryogenics* **2015**, *72*, 127−147.

(14) Kim, Y.; Lee, J.; An, N.; Kim, J. J. E. C. Advanced natural gas liquefaction and regasification processes: Liquefied natural gas supply chain with cryogenic carbon capture and storage. *Energy Convers. Manage.* **2023**, *292*, 117349.

(15) De Guido, G. Cryogenic CO2 capture from oxy-combustion flue gas by a hybrid distillation+ physical absorption process. *Chem. Eng. Res.* **2023**, *199*, 639−658.

(16) Lei, T.; Luo, K. H.; Hernandez Perez, F. E.; Wang, G.; Wang, Z.; Restrepo Cano, J.; Im, H. G. Study of CO_2 desublimation during cryogenic carbon capture using the lattice Boltzmann method. *J. Fluid Mech.* **2023**, *964*, A1.

(17) Sreenath, S.; Sam, A. A. Hybrid membrane-cryogenic CO_2 capture technologies: A mini-review. *Front. Energy Res.* **2023**, *11*, 1167024.

(18) Alsanousie, A. A.; Attia, A. E.; Elhelw, M.; Elsamni, O. A. Towards nearly zero emissions natural gas-fired power plants using cryogenic carbon dioxide capture technology. *International Journal of Greenhouse Gas Control* **2023**, *127*, 103928.

(19) Maqsood, K.; Mullick, A.; Ali, A.; Kargupta, K.; Ganguly, S. Cryogenic carbon dioxide separation from natural gas: a review based on conventional and novel emerging technologies. *Reviews in Chemical Engineering* **2014**, *30* (5), 453−477.

(20) Song, C. F.; Kitamura, Y.; Li, S. H. J. A. e. Evaluation of Stirling cooler system for cryogenic CO_2 capture. *Applied Energy* **2012**, *98*, 491−501.

(21) Hlavinka, M. W.; Hernandez, V. N.; McCartney, D. J. I. Proper interpretation of freezing and hydrate prediction results from process simulation. In *Proceedings of the Ocean Drilling Program*; Bryan Research & Engineering, 2006; Vol. *199*.

(22) Tuinier, M.; van Sint Annaland, M.; Kramer, G. J.; Kuipers, J. J. C. E. S. Cryogenic CO_2 capture using dynamically operated packed beds. *Chemical Engineering Science* **2010**, *65* (1), 114−119.
(23) Wilhelmsen, Øi.; Aasen, A.; Skaugen, G.; Aursand, P.; Austegard, A.; Aursand, E.; Gjennestad, M. A.; Lund, H.; Linga, G.; Hammer, M. Thermodynamic modeling with equations of state: present challenges with established methods. *Ind. Eng. Chem. Res.* **2017**, *56* (13), 3503−3515.
(24) Ali, A.; Abdulrahman, A.; Garg, S.; Maqsood, K.; Murshid, G. Application of artificial neural networks (ANN) for vapor-liquid-solid equilibrium prediction for CH_4-CO_2 binary mixture. *Greenhouse Gases: Science and Technology* **2019**, *9* (1), 67−78.
(25) Abdulrahman, A.; Ali, A.; Alfazazi, A. Synthesis and process parameter optimization of biodiesel from Jojoba oil using response surface methodology. *Arabian Journal for Science and Engineering* **2021**, *46* (7), 6609−6617.
(26) Bezerra, M. A.; Santelli, R. E.; Oliveira, E. P.; Villar, L. S.; Escaleira, L. A. Response surface methodology (RSM) as a tool for optimization in analytical chemistry. *Talanta* **2008**, *76* (5), 965−977.
(27) Ahmed, A.; Ali, A.; Mubashir, M.; Lim, H. R.; Khoo, K. S.; Show, P. L. Process optimization and simulation of biodiesel synthesis from waste cooking oil through supercritical transesterification reaction without catalyst. *Journal of Physics: Energy* **2023**, *5*, 024003.
(28) Pikaar, M. J. A study of phase equilibria in hydrocarbon-CO_2 systems. *PhD Thesis*, Imperial College London, 1959.
(29) Xiong, X.; Lin, W.; Jia, R.; Song, Y.; Gu, A. Measurement and calculation of CO_2 frost points in CH_4+ CO_2/CH_4+ CO_2+ N_2/CH_4+ CO_2+ C_2H_6 mixtures at low temperatures. *Journal of Chemical & Engineering Data* **2015**, *60* (11), 3077−3086.
(30) Agrawal, G.; Laverman, R. Phase behavior of the methane-carbon dioxide system in the solid-vapor region. *Advances in Cryogenic Engineering* **1974**, 327−338.

https://doi.org/10.1021/acsomega.4c01526
ACS Omega 2024, 9, 27214−27221